International Journal of Pharmaceutics 655 (2024) 124004

Contents lists available at ScienceDirect

International Journal of Pharmaceutics

journal homepage: www.elsevier.com/locate/ijpharm

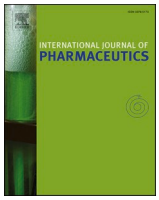

Nanobody-mediated targeting of zinc phthalocyanine with polymer micelles as nanocarriers

Bárbara Mesquita [a], Arunika Singh [a], Cèlia Prats Masdeu [a], Nienke Lokhorst [a], Erik R. Hebels [a], Mies van Steenbergen [a], Enrico Mastrobattista [a], Michal Heger [a,b,c], Cornelus F. van Nostrum [a,*], Sabrina Oliveira [a,d,*]

[a] Department of Pharmaceutics, Utrecht Institute for Pharmaceutical Sciences, Utrecht University, Utrecht, The Netherlands
[b] Jiaxing Key Laboratory for Photonanomedicine and Experimental Therapeutics, Department of Pharmaceutics, Jiaxing University, College of Medicine, Jiaxing, Zhejiang, PR China
[c] Membrane Biochemistry and Biophysics, Bijvoet Center for Biomolecular Research, Department of Chemistry, Utrecht University, Utrecht, The Netherlands
[d] Cell Biology, Neurobiology and Biophysics, Department of Biology, Science Faculty, Utrecht University, Utrecht, The Netherlands

ARTICLE INFO

Keywords:
Cancer treatment
Targeted nanomedicine
Stability
Biologicals
Active targeting
Nanobody

ABSTRACT

Photodynamic therapy (PDT) is a suitable alternative to currently employed cancer treatments. However, the hydrophobicity of most photosensitizers (e.g., zinc phthalocyanine (ZnPC)) leads to their aggregation in blood. Moreover, non-specific accumulation in skin and low clearance rate of ZnPC leads to long-lasting skin photosensitization, forcing patients with a short life expectancy to remain indoors. Consequently, the clinical implementation of these photosensitizers is limited. Here, benzyl-poly(ε-caprolactone)-b-poly(ethylene glycol) micelles encapsulating ZnPC (ZnPC-M) were investigated to increase the solubility of ZnPC and its specificity towards cancers cells. Asymmetric flow field-flow fractionation was used to characterize micelles with different ZnPC-to-polymer ratios and their stability in human plasma. The ZnPC-M with the lowest payload (0.2 and 0.4% ZnPC w/w) were the most stable in plasma, exhibiting minimal ZnPC transfer to lipoproteins, and induced the highest phototoxicity in three cancer cell lines. Nanobodies (Nbs) with binding specificity towards hepatocyte growth factor receptor (MET) or epidermal growth factor receptor (EGFR) were conjugated to ZnPC-M to facilitate cell targeting and internalization. MET- and EGFR-targeting micelles enhanced the association and the phototoxicity in cells expressing the target receptor. Altogether, these results indicate that ZnPC-M decorated with Nbs targeting overexpressed proteins on cancer cells may provide a better alternative to currently approved formulations.

1. Introduction

Photodynamic therapy (PDT) is a cancer treatment modality that combines a photoactivatable drug (photosensitizer, PS) with visible wavelength illumination to locally kill malignant cells. Upon illumination, the PS is activated and facilitates the production of reactive oxygen species (ROS), destroying the tumor cells that become incapable of coping with the acute hyperoxidative stress (Castano et al., 2004; Weijer, 2015). PDT offers several advantages over conventional cancer treatments, including a minimally invasive approach with negligible scarring, milder side effects, and spatiotemporal control over toxicity that is triggered only when the light and PS are colocalized, thereby limiting the pharmacodynamic effect to the tumor environment (Li, 2020; Van Straten, 2017). PDT has shown favorable outcomes in various cancer types, especially when applied in combination with surgery, chemotherapy, and/or immunotherapy (Hopper et al., 2004; Yu, 2023; Santos, 2018).

The success of PDT relies on the photochemical properties of the PS. The ideal photosensitizer should have strong absorption in the near-infrared wavelength range (~630–800 nm), high triplet state and ROS quantum yield, minimal dark toxicity, and a predominant specificity towards target tissue (Plaetzer, 2009). Since the first clinical trial with hematoporphyrin derivative for skin cancer, various photosensitizers have been approved for clinical use by different health agencies around the world (although not all by the same health agencies), including Photofrin (porfimer sodium), Foscan (temoporfin, mTHPC), Levulan

* Corresponding authors at: Department of Pharmaceutics, Utrecht Institute for Pharmaceutical Sciences, Utrecht University, Utrecht, The Netherlands.
E-mail addresses: c.f.vannostrum@uu.nl (C.F. van Nostrum), s.oliveira@uu.nl (S. Oliveira).

https://doi.org/10.1016/j.ijpharm.2024.124004
Received 13 December 2023; Received in revised form 11 March 2024; Accepted 14 March 2024
Available online 15 March 2024

(aminolevulinic acid hydrochloride), LUZ111 (Redaporfin), Metvix (methyl aminolevulinate), Laserphyrin (talaporfin), Tookad (padeliporfin), and Photosens (sulphonated aluminium phthalocyanine) (McFarland, 2020; Broadwater, 2021; Cramer et al., 2022). Unfortunately, none of these photosensitizers meet all the abovementioned criteria, and efforts have been made to both design new photosensitizers and to develop delivery strategies that enhance selective tumor photosensitization.

Zinc phthalocyanine (ZnPC) is a synthetic compound, structurally similar to porphyrins, that coordinates with zinc at the nitrogen atoms-containing core. Unlike porphyrins and chlorins, ZnPC has a high molar extinction coefficient at longer wavelengths (650 to 750 nm), i.e., greater optical penetration depth for ZnPC activation, higher triplet state quantum yields and longer triplet state lifetimes, and a more considerable singlet oxygen yield (Weijer, 2015; Allen et al., 2001; Roguin, 2019). However, ZnPC is very hydrophobic (logP of 8.5) (Weijer, 2015) and thus requires a suitable solubilizing agent for systemic administration. Liposomes encapsulating ZnPC (CGP55847) were developed by Ciga-Geigy in the 90 s and tested in a phase I/II clinical trial for the treatment of squamous cell carcinoma in the upper digestive tract before being abandoned (Ochsner, 1996; Isele, 1994). Although the motivation for this decision has not been disclosed, we speculate that insufficient stability of the liposomal formulation might have been one of the problems, leading to the accumulation of ZnPC in the skin as a result of extravasation from the dermal microcirculation, and consequent skin phototoxicity. Our speculation centers on the delivery system (non-PEGylated liposomes composed of 1-palmitoyl-2-oleoylphosphatidylcholine and 1,2-dioleoylphosphatidylserine) and not the ZnPC as the chief cause of the clinical trial termination. The nanoparticulate PS delivery system was therefore changed to micelles while the PS was retained.

Micelles are drug delivery systems composed of amphiphilic block copolymers that self-assemble in aqueous solution. These nanocarriers can improve solubilization of hydrophobic drugs such as ZnPC by stable entrapment in their hydrophobic core and consequently enhance drug availability after intravenous administration (Huang, 2012; Varela-Moreira, 2017; Park, 2021). Compared to liposomes, micelles have smaller size (<100 nm), which might further facilitate distribution and accumulation at the tumor site owing to the enhanced permeability and retention (EPR) effect (Ashford et al., 2021). In PDT, reducing the non-specific distribution of the PS can attenuate skin photosensitivity and improve therapeutic efficacy.

Most amphiphilic copolymers currently under investigation or in clinical cancer trials are composed of poly(ethylene) glycol (PEG), which forms the hydrophilic shell of nanoparticles (NPs) and is known to prolong circulation time by reducing protein adsorption and consequent recognition by macrophages (Klibanov, 1990; Suk, 2016). On the other hand, various hydrophobic blocks are being explored for the preparation of micelles, such as polyester (e.g., polylactic acid and poly-caprolactone), polyether, and poly(amino acid) chains (e.g., poly(glutamic acid), poly(aspartic acid), or poly(l-lysine)) (Cabral, 2018).

In this study, we investigated micelles composed of the block copolymer benzyl-poly(ε-caprolactone) (PCL)-*b*-PEG as nanocarrier for ZnPC. Previous research by our group has shown that PCL-PEG micelles are a suitable delivery system for mTHPC, as it exhibited both high loading capacity while maintaining high phototoxicity *in vitro* and a longer circulation time than free mTHPC in Balb/c nude mice (Liu, 2020). The stability of these PCL-PEG micelles was attributed to π-π stacking between the benzyl group and the aromatic mTHPC (Hofman, 2008). Considering that ZnPC possesses aromatic rings as well, we hypothesized that PCL-PEG micelles could also stably encapsulate this PS. Accordingly, and given the superior photophysical properties of ZnPC compared to mTHPC, we studied the stability of ZnPC loading in PCL-PEG micelles in a biologically relevant environment (human plasma) using asymmetric flow-field flow fractionation (AF4), and the phototoxicity in 2D and 3D models of human cancer. Moreover, to facilitate the interaction with cancer cells, micelles were decorated with a nanobody (Nb) targeting the hepatocyte growth factor receptor (MET) or the epidermal growth factor receptor (EGFR). Both tyrosine kinase receptors are frequently overexpressed in various tumor types (Raghav, 2012; Miyamoto, 2011), and several anti-MET and anti-EGFR targeted therapies have been approved to be used in the clinic (Min and Lee, 2022), and more are being developed, namely antibody drug conjugates (Yao et al., 2020; Lambert and Morris, 2017). Nbs are the variable domain of heavy chain-only antibodies found in camelids and are being explored as targeting ligands due to their small size (approximately 15 kDa), and thus ease of production, superior stability, and strong binding affinity compared to other antibody fragments (Muyldermans, 2013). Here, MET- and EGFR-targeted micelles (MET-TM and EGFR-TM, respectively) and non-targeted micelles (NTM) were characterized by dynamic light scattering and the extent of Nb conjugation was assessed by sodium dodecyl sulfate polyacrylamide gel electrophoresis (SDS-PAGE). The effect of MET-TM and EGFR-TM on the association with cells expressing the target receptor was compared to that of NTM by flow cytometry and compared with phototoxicity *in vitro*.

2. Materials and methods

References to supporting material are indicated with prefix 'S.'.

2.1. Materials

ε-Caprolactone, 4-nitrophenyl chloroformate (PNC), triethylamine (TEA), chloroform-d (99.8 atom % D), methoxy polyethylene glycol amine (PEG-NH_2, 2000 g/mol), lithium chloride, stannous octoate (Sn(Oct)2) and ZnPC (cat. # 341169, 97 % dye content) were purchased from Sigma-Aldrich (St. Louis, MO, USA). All organic solvents, including toluene, diethyl ether, tetrahydrofuran (THF), dichloromethane (DCM), and dimethylsulfoxide (DMSO) were obtained from Biosolve (Valkenswaard, the Netherlands). 2-Maleimidoethylamine hydrochloride (MAL-NH_2·HCl, RL-2780) was purchased from Iris Biotech (Marktredwitz, Germany). Amine PEG acetic acid, HCl salt (NH_2-PEG-COOH) was obtained from JenKem Technology USA (Plano, TX, USA). Phosphate buffered saline (PBS) 10 × solution (11.9 mM phosphate, 137 mM sodium chloride, 2.7 mM potassium chloride) was purchased from Fisher Bioreagents (Pittsburgh, PA, USA). L-cysteine hydrochloride and 1,4-dithiothreitol (DTT) were acquired from Sigma-Aldrich. Bolt 4 to 12 %, Bis-Tris, 1.0 mm, mini protein gels, Bolt 2-(N-morpholino)-ethanesulfonic acid (MES) SDS running buffer (20 ×), PageRuler prestained protein ladder, and Pierce Silver Stain Kit were obtained from Thermo Scientific (Waltham, MA, USA). Roswell Park Memorial Institute 1640 (RPMI 1640) medium, fetal bovine serum (FBS) (sterile filtered), trypsin EDTA solution (1 ×), antibiotic/antimycotic solution (100 ×), Dulbecco's PBS, tris(2-carboxyethyl)phosphine hydrochloride solution (TCEP) and *N*,*N*'-dicyclohexylcarbodiimide (DCC), 99 % were purchased from Thermo Scientific. Vivaspin 2 100,000 MWCO (PES membrane) was obtained from Sartorius Stedim Lab (Gloucestershire, UK).

2.2. Synthesis of polymers

2.2.1. Synthesis of benzyl-poly(ε-caprolactone)

Benzyl-poly(ε-caprolactone) (PCL) was synthesized as described elsewhere (Liu, 2020). Aiming at a degree of polymerization of approximately 23CL units, benzyl alcohol (1.00 mL, 10 mmol) and ε-caprolactone (24 mL, 221 mmol) were mixed in a round bottom flask and maintained at 130 °C. Under constant stirring, stannous octoate (Sn(Oct)2) (0.016 mL, 0.48 mmol) was added to the reaction mixture, which was then kept under a nitrogen atmosphere. The reaction was sampled every hour until the desired degree of polymerization was obtained as determined by ^{1}H NMR. Afterwards, the flask was brought to room temperature (RT) by passive cooling, and 20 mL of DCM was added to solubilize the formed PCL oligomers that were further

precipitated in 30-fold excess of cold diethyl ether (−20 °C). The precipitates were recovered via filtration and subsequently dried overnight under vacuum to obtain a white powder. The product was analyzed by ^{1}H NMR spectroscopy ($CDCl_3$): δ = 7.35 (b, aromatic protons, benzyl alcohol), 5.10 (s, C**H$_2$**O), 4.07 (m, CH$_2$**CH$_2$**O), 3.61 (t, CH$_2$**CH$_2$**OH), 2.32 (m, OC(O)**CH$_2$**), 1.65 (m, CH$_2$**CH$_2$**CH$_2$**CH$_2$**CH$_2$), 1.38 (m, CH$_2$CH$_2$**CH$_2$**CH$_2$CH$_2$).

2.2.2. Synthesis of benzyl-poly(ε-caprolactone)-p-nitrophenyl formate (PCL-PNF)

The PCL oligomers (0.5 g, 0.16 mmol) obtained from the previous reaction were dissolved in 2.5 mL of dry toluene in a round bottom flask. Subsequently, TEA (70 μL, 0.53 mmol) and PNC (0.11 g, 0.53 mmol) were added to the flask, and the reaction proceeded overnight at RT under constant magnetic stirring and a nitrogen atmosphere. The formed TEA·HCl precipitates were removed by centrifugation (2,600 × g for 4 min at RT), and the supernatant was dropped into 30-fold excess of cold diethyl ether (−20 °C) to induce polymer precipitation. The precipitates were recovered via centrifugation (2,600 × g for 5 min at RT) and subsequently dried overnight under vacuum. The product was analyzed by ^{1}H NMR spectroscopy ($CDCl_3$): δ = 8.29 (d, aromatic protons, PNF), 7.38 (m, aromatic protons, PNF), 7.35 (m, aromatic protons, benzyl alcohol), 5.11 (s, C**H$_2$**O), 4.31 (t, CH$_2$**CH$_2$**OC(O)O), 4.06 (m, CH$_2$**CH$_2$**O), 2.30 (m, OC(O)**CH$_2$**), 1.64 (m, CH$_2$**CH$_2$**CH$_2$**CH$_2$**CH$_2$), 1.4 (m, CH$_2$CH$_2$**CH$_2$**CH$_2$CH$_2$).

2.2.3. Synthesis of benzyl-poly(ε-caprolactone)-b- poly(ethylene glycol) methyl ether (PCL-PEG)

The above-obtained PCL-PNF (0.33 g, 0.1 mmol) and PEG-NH_2 (0.2 g, 0.1 mmol) were mixed in dry toluene, and the reaction was stirred overnight at RT under a nitrogen atmosphere. Afterwards, the polymer was precipitated in cold diethyl ether, recovered by centrifugation, and dried under vacuum as described above. To remove unreacted PEG-NH_2 and p-nitrophenol, the product was dispersed in deionized water and dialyzed (Spectra/Por 3 Dialysis Tubing, 3.5 kD MWCO, Thermo Scientific) for 2 d at 4 °C. The product was analyzed by ^{1}H NMR spectroscopy ($CDCl_3$): δ = 7.37 (m, aromatic protons, benzyl alcohol), 5.11 (s, C**H$_2$**O), 4.06 (m, CH$_2$**CH$_2$**O), 3.65 (m, PEG protons), 3.38 (s, O**CH$_3$**), 2.32 (m, OC(O)**CH$_2$**), 1.64 (m, CH$_2$**CH$_2$**CH$_2$**CH$_2$**CH$_2$), 1.4 (m, CH$_2$CH$_2$**CH$_2$**CH$_2$CH$_2$).

2.2.4. Synthesis of benzyl-poly(ε-caprolactone)-b-poly(ethylene glycol)-carboxylic acid (PCL-PEG-COOH)

TEA (205 μL, 1.4 mmol) and HCl·NH_2-PEG-COOH (0.15 g, 0.07 mmol) were mixed in 500 μL of dimethylformamide (DMF) and stirred for 1 h. Next, the PCL-PNF (0.21 g, 0.07 mmol; section 2.2.2) was dissolved in 2 mL of dry toluene and added to the reaction mixture, which was kept at RT for 2 d. Afterwards, the polymer was precipitated in cold diethyl ether, recovered by centrifugation, and dried under vacuum as described previously. The product was analyzed by ^{1}H NMR spectroscopy ($CDCl_3$): δ = 7.37 (m, aromatic protons, benzyl alcohol), 5.11 (s, C**H$_2$**O), 4.06 (m, CH$_2$**CH$_2$**O), 3.65 (m, PEG protons), 2.32 (m, OC(O)**CH$_2$**), 1.64 (m, CH$_2$**CH$_2$**CH$_2$**CH$_2$**CH$_2$), 1.4 (m, CH$_2$CH$_2$**CH$_2$**CH$_2$CH$_2$).

2.2.5. Synthesis of benzyl-poly(ε-caprolactone)-b-poly(ethylene glycol)-maleimide (PCL-PEG-MAL)

The PCL-PEG-COOH (0.10 g, 0.02 mmol), MAL-NH_2·HCl (3.5 mg, 0.025 mmol) and TEA (103 μL, 0.7 mmol) were mixed in 500 μL of DCM under magnetic stirring. After 1 h, *N,N′*-dicyclohexylcarbodiimide (DCC) (10 mg, 0.031 mmol) was added to the reaction mixture, which proceeded overnight at RT. Next, the polymer was precipitated in cold diethyl ether, recovered by centrifugation (2,600 × g for 5 min at RT), and dried overnight under a stream of nitrogen. To remove DCC and unreacted MAL-NH_2, gel permeation chromatography was performed in 1:1 DCM:methanol. The product was analyzed by ^{1}H NMR spectroscopy ($CDCl_3$): δ = 7.37 (m, aromatic protons, benzyl alcohol), 6.71 (s, maleimide protons), 5.11 (s, C**H$_2$**O), 4.06 (m, CH$_2$**CH$_2$**O), 3.65 (m, PEG protons), 2.32 (m, OC(O)**CH$_2$**), 1.64 (m, CH$_2$**CH$_2$**CH$_2$**CH$_2$**CH$_2$), 1.4 (m, CH$_2$CH$_2$**CH$_2$**CH$_2$CH$_2$).

2.3. Polymer characterization

2.3.1. Proton nuclear magnetic resonance

Proton nuclear magnetic resonance (^{1}H NMR) spectra were recorded using an Agilent 400-MR NMR spectrometer (Agilent Technologies, Santa Clara, CA, USA). Residual solvent peak of $CDCl_3$ (δ = 7.26 ppm) was used to calibrate ^{1}H chemical shifts. Peak multiplicity was designated as s (singlet), d (doublet), and m (multiplet).

The degree of polymerization of the caprolactone chain was determined from the ratio of the integral of the CH_2 protons of the ε-CL units (4.06 ppm, CH$_2$**CH$_2$**O) to the CH_2 protons of the benzyl alcohol (5.10 ppm, C**H$_2$**O). The number-average molecular weight (Mn) of the PCL-PEG polymer was determined by ^{1}H NMR and determined from the calculated number of caprolactone units and assuming 45 ethylene oxide units.

2.3.2. Gel permeation chromatography

The weight- and number average molecular weights (Mw and Mn, respectively) of PCL-PEG and PCL-PEG-MAL polymers were determined by gel permeation chromatography (GPC; Alliance 2695 System, Waters, Milford, MA, USA), equipped with two PLgel Mesopore columns (300 × 7.5 mm, including a guard column, 50 × 7.5 mm). DMF containing 10 mM LiCl was used as the eluent at a flow rate of 1.0 mL/min at 65 °C. A differential refractive index (RI) detector was used to record the chromatograms. The polymers were dissolved in DMF containing 10 mM LiCl at 3 mg/mL and 50-μL samples were injected onto the column. A calibration curve was prepared using narrow poly(ethylene glycol) standards (PSS, Mainz, Germany) ranging from 430 to 26,100 g/mol, and the Mw and Mn of the PCL-PEG block copolymers were calculated using Empower 32 software.

2.3.3. Differential scanning calorimeter

The thermal properties of PCL-PEG was determined using a differential scanning calorimeter (TA Discovery Series, TA Instruments, Newcastle, DE, USA). Indium standard (TA Instruments) was used for calibration. Briefly, 5–10 mg of the sample was subjected to a heat-cool-heat cycle, moving from − 80 °C to 150 °C at a heating and cooling rate of 3 °C/min.

2.4. Production of MET- and EGFR-targeting nanobodies

MET-targeted and EGFR-targeted Nb (MET-Nb and EGFR-Nb, respectively) were produced and purified as described in (Mesquita, 2022). Nb concentration was determined using absorbance at 280 nm (Nanodrop One, Thermo Scientific) and a molar extinction coefficient of 37,025 $M^{-1}cm^{-1}$ for MET-Nb and 37,360 $M^{-1}cm^{-1}$ for EGFR-Nb (calculated with ProtParam tool in Expasy).

2.5. Preparation of ZnPC-loaded polymeric micelles and nanobody conjugation

The ZnPC-loaded polymeric micelles (ZnPC-M) were prepared at different payloads (0.2, 0.4, and 0.6 % w/w) by the film hydration method adapted from (Liu, 2020). In detail, 10 mg of PCL-PEG was dissolved in 1 mL of DCM in a round-bottom flask. Subsequently, a specific volume of ZnPC in THF was added depending on the target ZnPC payload. The solvents were removed in a rotary evaporator at 60 °C and dried under a stream of nitrogen gas for 30 min. The polymer film was hydrated with PBS (pH = 7.4) in a water bath at 50 °C to achieve a final polymer concentration of 10 mg/mL. The product was manually extruded 2 times through a 0.2-μm filter (Phenex-NY syringe filters, 4-mm diameter, Phenomenex, Torrance, CA, USA).

For preparing nanobody-conjugated micelles, PCL-PEG-MAL was included at 10 % w/w at the expense of PCL-PEG, and the same preparation method as described above was used. For the conjugation of the MET-Nb or EGFR-Nb onto the surface of micelles, Nbs in PBS were reduced with TCEP at a Nb:TCEP molar ratio of 1:200 and incubated for 5 min at RT. Next, TCEP was removed by buffer exchange to PBS (pH = 7.4) with Zeba spin desalting columns (7 kDa MWCO, Thermo Scientific). MET-Nb or EGFR-Nb were mixed with the micelles at a molar ratio of 4.5:100 Nb:PCL-PEG-MAL and incubated in an orbital shaker for 2 h at RT and overnight at 4 °C. To quench the unreacted maleimide groups, a cysteine solution at 100 × the molar concentration of PCL-PEG-MAL was prepared in PBS (pH = 7.4), added to the micelle dispersion (1:10 dilution), and shaken for 2 h at RT. NTMs were prepared by blocking the maleimide groups with cysteine as described for the MET-TMs and EGFR-TMs. To remove non-conjugated Nbs and concentrate the sample, micelles were centrifugated 3 x at 3,000 × g over Vivaspin 100-kDa columns (Sartorius).

2.6. Characterization of micelles

2.6.1. Dynamic and electrophoretic light scattering

The hydrodynamic diameter and polydispersity of the micelles was measured at a fixed scattering angle of 173° using a ZetaSizer Nano S (Malvern Instruments, Malvern, UK). Micelles were diluted 1:100 v/v in PBS (pH = 7.4). The ζ-potential of the micelles was measured at 1:1000 in 10 mM HEPES (pH = 7.4) using a Zetasizer Nano Z.

2.6.2. Absorbance spectroscopy

ZnPC loaded in the micelles was quantified by ultraviolet–visible light spectroscopy at 674 nm against a calibration curve of ZnPC in DMSO (UV-2450 spectrophotometer, Shimadzu, Kyoto, Japan). Briefly, micelles were diluted 1:4 in PBS and then dissolved in DMSO at 1:10 v/v. ZnPC standards (0.25 μM to 4 μM) were prepared in DMSO and spiked with 10 % v/v of PBS (pH = 7.4). The absorption spectrum of ZnPC-M was recorded. ZnPC-M were dispersed in aqueous buffer or dissolved in DMSO at a final concentration of 4 μM ZnPC.

2.6.3. SDS-PAGE

SDS-PAGE was performed to confirm MET-Nb and EGFR-Nb conjugation to the micelles. In short, 10 μL of sample was mixed with 4 × SDS sample buffer (1:4 v/v, 30 μL total sample volume) and PBS and incubated at 90 °C for 10 min. After cooling down, the samples and the PageRuler Plus Prestained Protein Ladder (10 to 250 kDa) were loaded onto an SDS-PAGE gel (Bolt, 4–12 % Bis-Tris Plus, Invitrogen | Thermo Scientific) and run at 100 V for 50 min, employing 1 × MES buffer as running buffer. Afterwards, the gel was stained with silver staining (Pierce Silver Stain Kit, Thermo Fisher) and scanned with a ChemiDoc Imaging System (BioRad, Hercules, CA, USA).

2.6.4. Asymmetric flow field flow fractionation

AF4 was performed using an AF2000 system (Postnova Analytics, Landsberg am Lech, Germany), equipped with an absorbance 2487 and fluorescence 2475 detector (Waters), a PN3150 refractive index (RI) detector (Postnova Analytics), a PN3621 multi-angle light scattering (MALS) detector with a 488-nm laser and 21 detection angles (Postnova Analytics), and a Zetasizer Nano S (Malvern Panalytical). The separation channel included a 500-μm spacer and a regenerated cellulose membrane with a 10-kDa cutoff (Postnova Analytics). PBS (pH = 7.4) filtered with OmiporeTM 0.1 v PTFE membrane (Merck Millipore, Burlington, MA, USA) was used as eluent. Next, 60 μL of ZnPC-M (at 5 mg/mL of PCL-PEG in PBS (pH = 7.4)) was injected into the channel with an autosampler, focused for 7 min at a focus flow rate of 4.3 mL/min and cross-flow of 4 mL/min, and separated using the elution profile according to Table 1. NovaFFF AF2000 software was used to process and analyze the raw data. MALS data were fitted with a sphere model.

Table 1
Elution profile used for separation of ZnPC-M in AF4.

Elution Step	Time (min)	Crossflow (mL/min)	Type	Exponent
1	5	4.00	constant	–
2	30	4.00 to 0.1	power	0.2
3	30	0.1 to 0.05	power	0.8
4	20	0.05	constant	–
5	10	0.00	constant	–

2.7. Stability of ZnPC-M in human plasma

ZnPC-M at 0.2, 0.4, and 0.6 % w/w ZnPC were mixed with human plasma (Human Plasma 3.8 % NaCit Gender Pooled, BioIVT, New York, NY, USA) at 1:2 v/v and incubated for different durations at 37 °C under shaking (400 rpm). Immediately after mixing and at 2, 6, and 24 h, samples were analyzed by AF4 using the same equipment as described in section 2.5.4. Thirty μL of sample was injected into the channel with an autosampler, focused for 7 min at a focus flow rate of 3.3 mL/min and cross-flow of 3 mL/min, and separated using the elution profile according to Table 2. Bovine serum albumin (BSA, Sigma-Aldrich), high-density lipoprotein (HDL, cat # 361–10, Medix Biochemica, Espoo, Finland) and low-density lipoprotein (LDL, cat # 360–10, Medix Biochemica) were run as standards using the same method.

ZnPC retention in ZnPC-M was quantified by collecting the micelle fraction of samples incubated with human plasma for 1 min and 24 h. Briefly, micelles were injected into the AF4 channel as described above and the fractions eluting between 42 and 56 min were collected into glass vials using a fraction collector. Next, the collected fractions were concentrated 10 x by centrifugation at 5,000 x g with a Vivaspin 3-kDa column (Sartorius). Afterwards, the samples were dissolved 1:10 in DMSO and the fluorescence intensity of ZnPC was measured with an FP-8300 spectrofluorometer (Jasco, Tokyo, Japan) at excitation/emission wavelengths of 660/685 nm. The ratio between the ZnPC signal intensity at 24 h and 1 min samples was calculated to determine ZnPC retention in the micelles.

2.8. Cell culture

The human extrahepatic bile duct carcinoma TFK1 cell line (ACC 344) and EGI1 (ACC 385) were purchased from Leibniz Institute DSMZ-German Collection of Microorganisms and Cell Cultures (Braunschweig, Germany). The epidermoid carcinoma A431 cell line (CRL-1555) was obtained from American Type Culture Collection (ATCC, Manassas, VA, USA). Cells were cultured in RPMI 1640 (cat. # 11875093, Thermo Scientific) supplemented with 10 % FBS and maintained at 37 °C in a humidified atmosphere composed of 95 % air and 5 % CO_2 (standard culture conditions).

2.8.1. Preparation of TFK1 spheroids

TFK1 spheroids were prepared by liquid overlay in a 96-wells flat bottom plate following optimization in a trial and error pilot. Briefly, a thin layer of 50 % v/v Matrigel in PBS was added to each well and incubated at 37 °C for 1 h. Next, 4 x 10^3 cells in RPMI supplemented with 10 % FBS were added on top and incubated for 6 d with medium refreshment every 2 d.

Table 2
Elution profile used for separation of ZnPC-M in AF4.

Elution Step	Time (min)	Crossflow (mL/min)	Type	Exponent
1	20	3.00	constant	–
2	30	3.00 to 0.1	power	0.2
3	30	0.1 to 0.05	power	0.8
4	20	0.05	constant	–
5	5	0.00	constant	–

2.9. Expression of MET and EGFR

TFK1, EGI1, and A431 cells (100,000 cells per sample) were fixed for 15 min with 4 % paraformaldehyde (PFA) and blocked with PBS containing 1 % bovine serum albumin (BSA). To quantify MET expression, cells were incubated with 50 μL of the fluorescently labeled antibody (PE-conjugated anti-Met (c-Met) antibody, cat. # ab279587, Abcam, Cambridge, UK) diluted 1:200 in blocking buffer for 45 min at RT, washed 3 x with PBS with 1 % BSA, and resuspended in 100 μL of blocking buffer. To quantify EGFR expression, cells were incubated with 50 μL of the primary antibody against EGFR diluted 1:300 in blocking buffer (cetuximab, from local pharmacy) for 45 min at RT, washed 3 x with PBS with 1 % BSA, and incubated with 50 μL of the secondary antibody diluted 1:250 in blocking buffer (goat anti-human Alexa 488-labeled IgG, cat. # A-11013, Invitrogen, Carlsbad, CA, USA) for 45 min at RT. Next, cells were washed, resuspended in 100 μL of blocking buffer, and transferred to a 96-wells plate. Fluorescence intensity was measured with a flow cytometer (Canto II, BD Biosciences, Franklin Lakes, NJ, USA) using the 488-nm laser line in combination with a 530/30 nm and 585/42 nm emission filter. At least 10,000 events were collected per sample in the gated region. Mean fluorescence intensity was calculated using FlowLogic software (Inivai Technologies, Mentone, Australia).

2.10. Dark toxicity and phototoxicity of ZnPC-loaded micelles

TFK1, EGI1, and A431 cells were seeded at a density of 0.8×10^4, 1.2×10^4, and 1.2×10^4 cells per well, respectively, in a 96-wells plate. After 24 h, cells were incubated for 6 h with formulations dispersed in fully supplemented RPMI (10 % FBS and 2 % penicillin and streptomycin (P/S, Gibco Antibiotic-Antimycotic, cat # 15240062, Thermo Fisher)). After incubation and washing, cells were illuminated at 5 mW/cm^2 for 40 min using a bespoke LED device (1 LED per well, 650 ± 20 nm), accounting for a cumulative radiant exposure of 12 J/cm^2 in concordance with previous *in vitro* studies (Dias, 2021; Dias, 2022). The radiant exposure was measured with an optometer P9710 (Te Lintelo Systems, Zevenaar, the Netherlands). Cell viability was measured 16 h post-illumination using an MTS assay (CellTiter 96 AQueous One Solution Cell Proliferation Assay, cat # G3581, Promega, Masison, WI, USA) following the manufacturer's instructions. To determine dark toxicity, cells were exposed to the same concentration of ZnPC-M but were not illuminated.

For TFK1 spheroids, cells were incubated for 24 h and illuminated following the same procedure as described above. Cell viability was measured 16 h post-illumination with CellTiter-Glo 3D Cell Viability Assay (cat # G9681, Promega).

2.11. Generation of singlet oxygen

ZnPC-M (0.2, 0.4, and 0.6 % w/w ZnPC) were diluted to 25 μM ZnPC in RPMI supplemented with 10 % FBS. Singlet Oxygen Sensor Green (SOSG; Molecular Probes, Eugene, OR, USA) was added to the solutions at 10 μM final concentration. Fluorescence intensity was measured with an FP-8300 spectrofluorometer (Jasco) at an excitation/emission wavelength of 504/525 nm before and after 10-min illumination at 5 mW/cm^2 with a LED device.

2.12. Cell association of non-targeted and MET-/EGFR-targeted micelles

TFK1, EGI1, and A431 cells were seeded at a density of 3.5×10^4, 3.5×10^4, and 3×10^4 cells per well, respectively, in a 48-wells plate. The next day, cells were exposed to NTM, MET-ML, and EGFR-TM dispersed in RMPI with 10 % FBS and 2 % P/S at 2 μM of ZnPC for 1 h and 6 h at standard culture conditions. A competition group with free Nb was included in the assay. In this case, cells were first incubated for 15 min with 1 μM of MET-Nb or EGFR-Nb, and then MET-TM and EGFR-TM, respectively, were added on top. For NTM, EGFR-Nb was used as control. After incubation, cells were washed 3 x to remove unbound micelles, detached with 100 μL/well of Accutase (cat. # A6964, Sigma-Aldrich), transferred to a round-bottom plate, and fixed with 4 % PFA for 15 min. ZnPC association with cells was measured by flow cytometry (Canto II) using the 633-nm laser line and a 660/20 filter. At least 10,000 events were collected in the gated region per sample. Mean fluorescence intensity was determined for each sample and corrected for background signal intensity of non-treated cells using FlowLogic software.

2.13. Statistical analysis

Statistical analysis was performed with GraphPad Prism 10 (GraphPad Software, San Diego, CA, USA). Kruskal-Wallis test (nonparametric test) was used to compare the association of MET-TM, EGFR-TM, and NTM with cells. A P-value of ≤ 0.1 was considered statistically significant. The highest P-value was noted in the results table.

3. Results and discussion

3.1. Characterization of ZnPC-loaded micelles

The PCL-PEG was synthesized as depicted in Fig. S1. Previous work from our group had shown that a degree of polymerization of 23 units improved the stability of PCL-PEG micelles loaded with mTHPC compared to lower degrees of polymerization (9 and 15) (Liu, 2020). We therefore aimed at photosensitizer micellization using the longer PCL chains. The degree of polymerization of the PCL chain was approximately 29 units as determined by ^{1}H NMR (Figs. S2 and S3, Table S1). The physicochemical properties of PCL-PEG copolymers, including Mw, polydispersity index and thermal behavior, as determined by ^{1}H NMR, GPC, and DSC are summarized in Figs. S2, S3, and S4 and Table S1.

To study the effect of ZnPC loading on the properties of micelles, PCL-PEG micelles were prepared encapsulating ZnPC at different payloads (0.2, 0.4, and 0.6 % w/w) and characterized using different techniques (Fig. 1). AF4 is an analytical technique that allows the separation of particles based on size and an in-depth characterization of NPs is achieved by using an in-line multidetector system. As shown in Fig. 1A, the spectroscopic ZnPC peak at λ_{abs} 674 nm (top graphic) overlaps with the micelle peak detected by DLS and MALS (middle and bottom graphic) and increases in proportion to the ZnPC payload, indicating successful encapsulation of ZnPC. For the three formulations, narrow fractogram peaks were detected by AF4-coupled DLS, attesting to the monodispersity of the samples with an average hydrodynamic radius (Rh) of approximately 23 nm. Batch-mode DLS yielded a slightly larger diameter of 30 nm as compared to AF4-coupled DLS (Fig. 1B). The performance of DLS is improved by fractionation with AF4 because larger particles at low percentage in the dispersion have less influence on the average NP size, which explains the lower Rh obtained with AF4-coupled DLS (Bhattacharjee, 2016; Wagner, 2014). Moreover, this method gives a more accurate determination of particle size distribution, which is essential for quality control. The average gyration radius (Rg) determined by MALS was also similar for all ZnPC-M and, in combination with the Rh, provides indirect information on the particle shape by the calculation of the Rg/Rh ratio (i.e., shape factor). As indicated in the table insert in Fig. 1B, the shape factor varied between 0.69 and 0.81. Homogeneous hard spheres have a shape factor of approximately 0.778, while lower values are indicative of NPs with a dense core surrounded by a lighter shell (Quattrini, 2021). Therefore, these results confirmed that the ZnPC-M have a core–shell structure. The ZnPC-M had a slightly negative charge of approximately − 10 mV (Fig. 1B), which is consistent with other measurements of PCL-PEG micelles (Liu, 2020).

The absorption spectrum of ZnPC-M in PBS exhibited lower absorptivity at the photosensitizer's absorption maximum (674 nm)

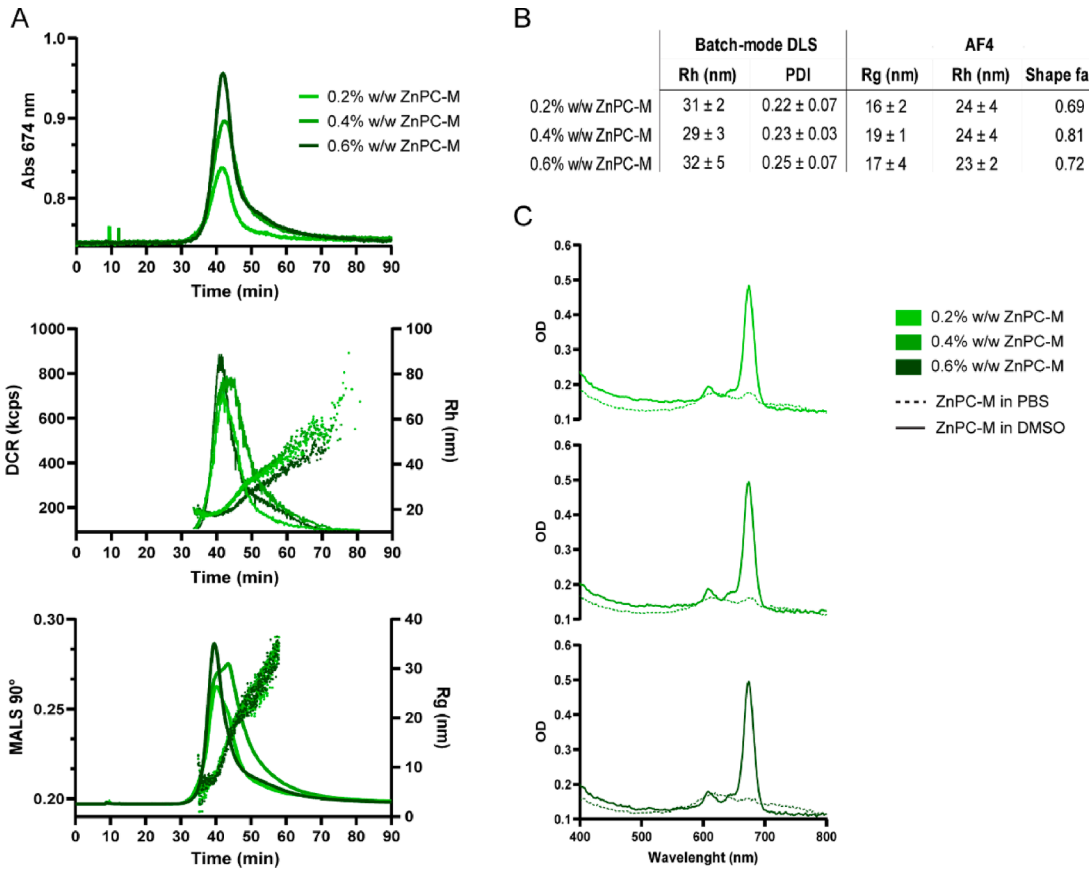

	Batch-mode DLS		AF4			Zetasizer
	Rh (nm)	PDI	Rg (nm)	Rh (nm)	Shape factor	ζ potential (mV)
0.2% w/w ZnPC-M	31 ± 2	0.22 ± 0.07	16 ± 2	24 ± 4	0.69	-8.2 ± 2.4
0.4% w/w ZnPC-M	29 ± 3	0.23 ± 0.03	19 ± 1	24 ± 4	0.81	-8.3 ± 0.8
0.6% w/w ZnPC-M	32 ± 5	0.25 ± 0.07	17 ± 4	23 ± 2	0.72	-11.8 ± 2.9

Fig. 1. ZnPC payload effects on the physicochemical properties of micelles. **(A)** Asymmetric flow field flow fractionation (AF4) fractograms of ZnPC-M using the ground state absorption maximum at 674 nm (top graph), derived count rate (DCR, solid lines in middle graphs), and hydrodynamic radius (Rh, scattered points in middle graph) from DLS; and multi-angle light scattering (MALS, solid line in bottom graph) at 90° and gyration radius (Rg, scattered points in bottom graph). **(B)** Table with ZnPC-M properties as determined by batch-mode DLS, AF4-coupled MALS and DLS, and electrophoretic light scattering. **(C)** Absorption spectrum of 4 μM ZnPC-M (0.2, 0.4 and 0.6 % w/w are represented by increasing shades of green, respectively) dispersed in aqueous buffer (dashed line) and dissolved in DMSO (solid line). (For interpretation of the references to color in this figure legend, the reader is referred to the web version of this article.)

compared to equimolar, micelle-derived, monomeric ZnPC in DMSO (Fig. 1C). This indicates that the ZnPC resides in aggregated state inside the micelles, which alters the vibronic transitions of the chromophore's delocalized π-electrons responsible for the metallated phthalocyanine's Q-band. Restoration of the 674-nm Q-band occurs upon ZnPC-M solubilization in DMSO. Photosensitizer aggregation was observed for all the assayed payloads, however at higher loadings the photogeneration of singlet oxygen was the lowest (Fig. S5). Others have described aggregation of ZnPC in different micellar nanoformulations, albeit at higher payloads (2 to 5 % w/w) (Obata, 2018; Obata, 2021). Similarly, ZnPC di- and multimerization has been observed in liposomes, typically at a photosensitizer:phospholipid ratio between 0.003 and 0.005 (Broekgaarden, 2014; Nunes et al., 2004). Master *et al.* have also observed that increasing silicon phthalocyanine in PCL-PEG (4.3 kDa) micelles to a certain threshold affects the production of singlet oxygen (Master, 2012), which has been echoed in studies on liposomal ZnPC in terms of molar absorptivity, fluorescence emission, ROS generation, and photo-induced biomolecule oxidation (Broekgaarden, 2014).

3.2. Stability of ZnPC-M in human plasma

The stability of ZnPC-M in blood was determined by incubating ZnPC-M with 50 % v/v human plasma for different durations and following the distribution of the ZnPC fluorescence signal between micelles and plasma components using AF4. Fig. 2A shows the fractograms based on MALS, DLS, and fluorescence spectroscopy of the 3 formulations incubated with plasma for 1 min, 2 h, 6 h, and 24 h. In both the MALS and DLS chromatograms, a broadening and/or a shift of the micelle peak to the right on the *x*-axis was detected at the 24 h time point, indicating a slight increase in the Rg and Rh of the ZnPC-M. This is probably due to adsorption of plasma proteins to the NP surface, which can only be partly deterred by the PEG layer (Bilardo, 2022).

ZnPC fluorescence intensity (FI) at 1 min overlapped with the micelle peak (at approximately 45–60 min). However, starting at 2 h incubation, the ZnPC signal was also detected between 30 and 40 min (Fig. 2A, bottom panel). The FI at 30–40 min elution time did not increase further, and for the 0.2 and 0.4 % w/w ZnPC-M there was even a small reduction at 24 h. AF4 chromatograms recorded with the absorbance detector set at 674 nm showed an increase in ZnPC signal intensity in the micelle peak over time for the 0.6 % w/w ZnPC-M, which can be attributed to a decrease in aggregation-induced quenching by the release of ZnPC (Fig. S6). To determine which components of human plasma the ZnPC was transferred to, standards of BSA, HDL, and LDL were run separately on AF4 using the same method. As depicted in Fig. S7, a corresponding peak was found in the human plasma sample at 280 nm for BSA and for MALS 90° for HDL and LDL. With these standards, it was possible to conclude that ZnPC was transferred specifically to HDL, which eluted between 30 and 40 min. The incubation of ZnPC dissolved in DMSO with plasma also resulted in association of ZnPC with HDL and LDL (Fig. S8). The preferential distribution of ZnPC to HDL and/or LDL from ZnPC-loaded liposomes and ZnPC non-covalently bound to BSA was reported previously (Larroque et al., 1996; Polo, 1992). It should be noted, though, that the ZnPC-carrying liposomes were not PEGylated (Polo, 1992); particle-bioparticle interactions were therefore unhampered due

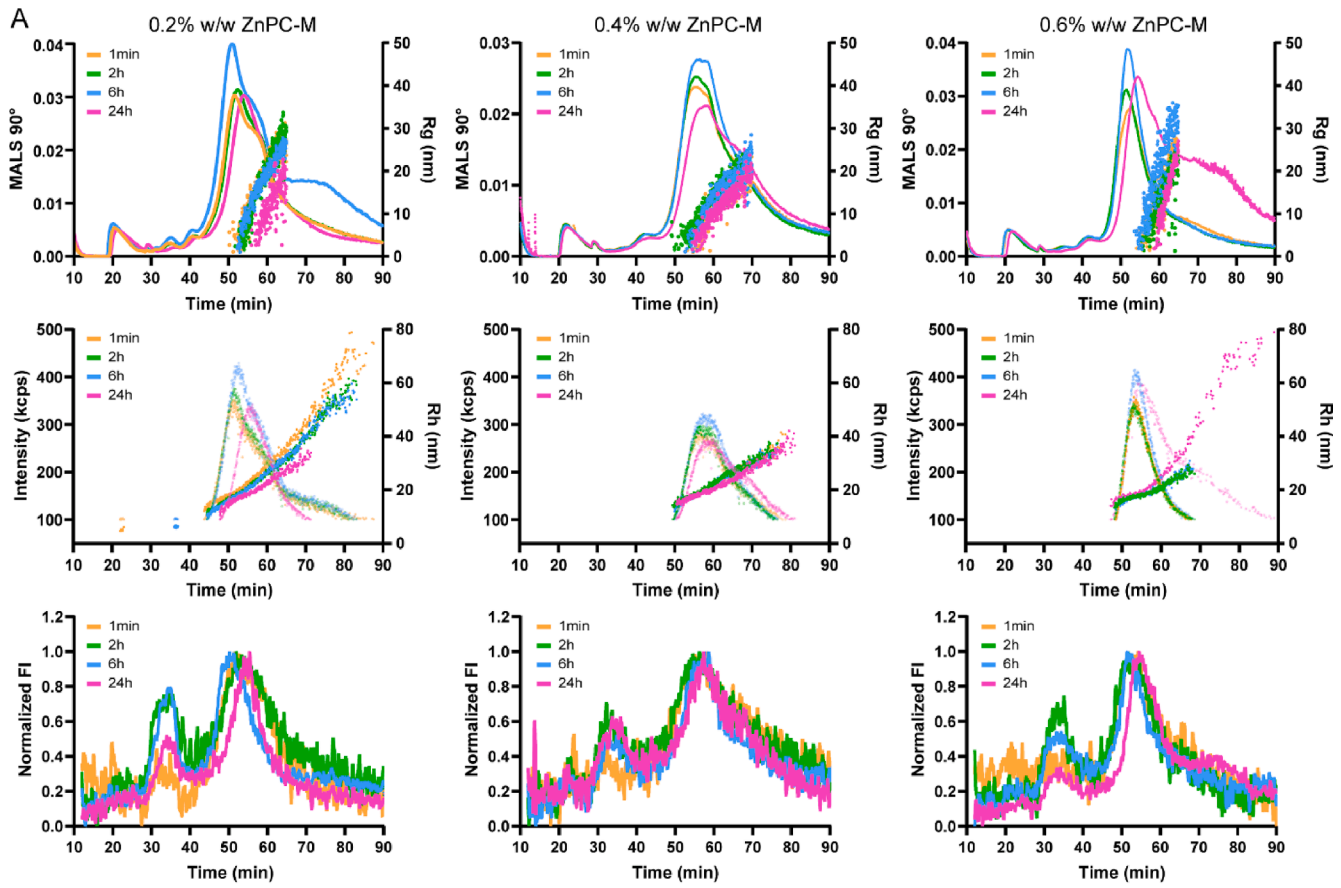

B

	Ratio $ZnPC_{24h}/ZnPC_{1min}$
0.2% w/w ZnPC-M	1.01 ± 0.25
0.4% w/w ZnPC-M	0.98 ± 0.02
0.6% w/w ZnPC-M	0.81 ± 0.19

Fig. 2. The effect of ZnPC payload (from left to right: 0.2 %, 0.4 %, and 0.6 % w/w) on the stability of ZnPC-M incubated with 50 % v/v human plasma for 1 min, 2 h, 6 h, and 24 h at 37 °C. **(A)** Asymmetric flow field flow fractionation (AF4) fractograms of ZnPC-M show MALS 90° (solid line) and Rg (scattered points) in the top panels, DCR (light color) and Rh (bold color) in the middle panels, and normalized fluorescent intensity (FI) at excitation/emission of 674/685 nm in the bottom panels. **(B)** Ratio of ZnPC in the micelles between 24 h and 1 min incubation with 50 % v/v human plasma calculated by measuring ZnPC fluorescence upon dissolving the collected fractions in DMSO (mean ± SD, N = 3).

to lacking steric hindrance.

To quantify the amount of ZnPC retained in the micelles while avoiding quenching caused by the aggregation of ZnPC in the micellar core, eluted micelle fractions in the 1 min and 24 h samples were collected and ZnPC was quantified by fluorescent spectroscopy after dissolving the samples in DMSO. The table from Fig. 2B shows the ratio of ZnPC between 24 h and 1 min incubation in diluted plasma for the three formulations. The 0.2 and 0.4 % w/w ZnPC-M showed the highest retention of ZnPC (almost 100 %), with the 0.4 % ZnPC-M exhibiting more intersample consistency. The 0.6 % w/w ZnPC-M formulation released approximately 20 % of the cargo during the course of 24 h. The method for precise quantification of ZnPC transfer in each fraction may be optimized by coupling a detector for inductively coupled plasma-mass spectrometry (ICP-MS) to AF4. ICP-MS is an elemental analysis technique with lower detection limits than fluorescence spectroscopy. Nevertheless, the current setup was sufficient to ascertain the uncoupling of ZnPC from its delivery vehicle under quasi-biological circumstances.

AF4 has been previously employed by our group to study qualitatively the stability of PS-loaded micelles, in the case with mTHPC, and a positive correlation between the AF4 stability results and the circulation time of micelles and mTHPC alike in a mouse model was observed (Liu, 2020). In this study with ZnPC-M, extra effort was made to quantify the release of the PS from the micelles, and we found that the ZnPC-M are stable in human plasma up to 24 h, particularly at 0.4 % w/w ZnPC-M. Accordingly, 0.4 % w/w ZnPC-M are expected to circulate long enough for ZnPC to specifically accumulate in the tumor, notwithstanding any destabilizing or elimination effects imparted by plasma.

3.3. *Dark toxicity and phototoxicity of ZnPC-M*

The capacity of ZnPC-M to induce toxicity upon illumination was studied in two human cholangiocarcinoma cell lines (TFK1 and EGI1) and a human epidermoid carcinoma cell line (A431). As shown in Fig. 3A, the three cell lines were differentially sensitive to ZnPC-M, with the order from the highest to the lowest LC_{50} being TFK1 > EGI1 > A431. At the same concentrations, no toxicity was observed when TFK1 cells were not illuminated (Fig. S9). Interestingly, increasing the amount of ZnPC loaded into the micelles did not proportionally affect their phototoxicity. Contrary to expectations, the highest loaded ZnPC-M (0.6 % w/w) induced the lowest toxicity in all cell lines. Assuming that the uptake rate is proportional to the ultimately intracellular micelle

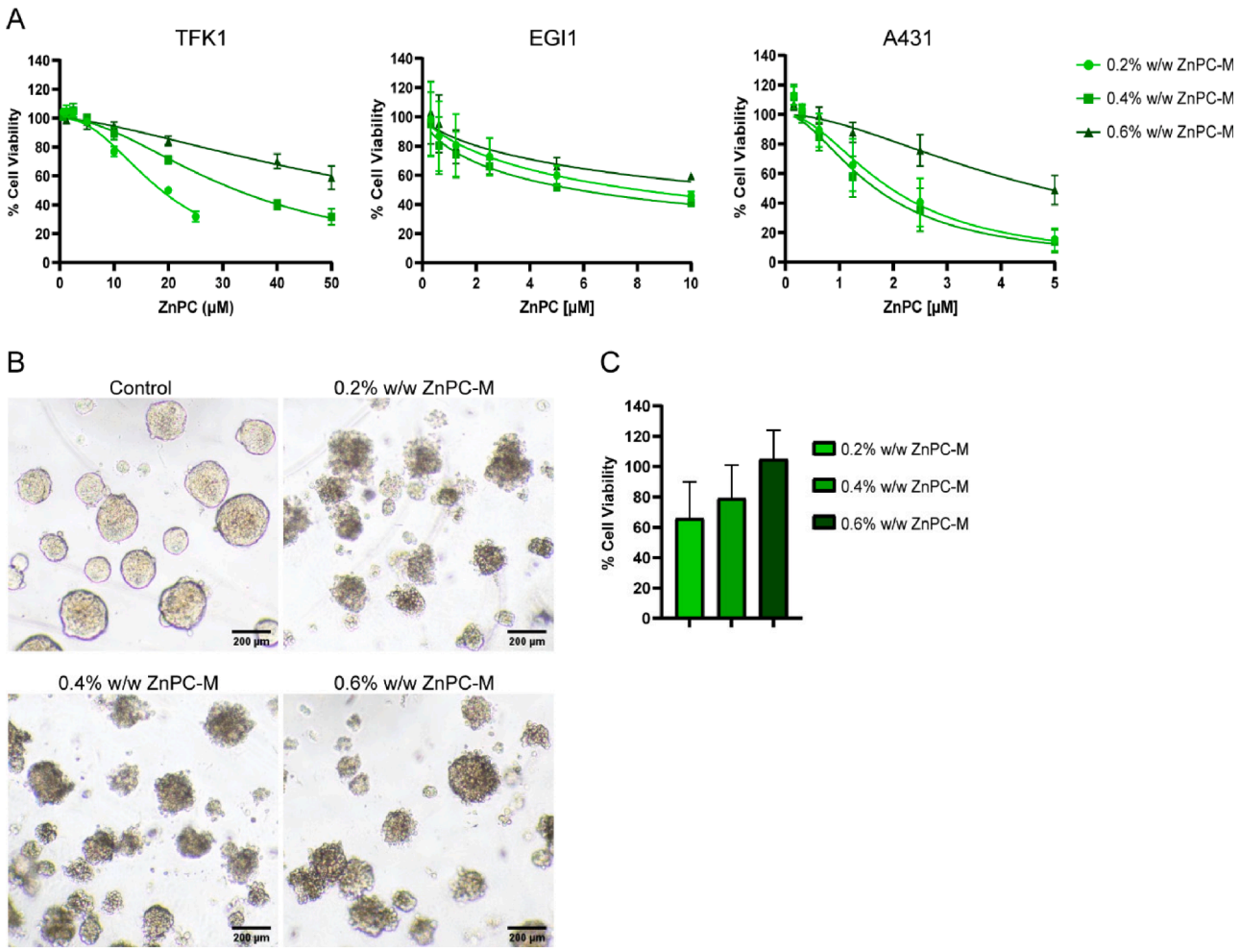

Fig. 3. The effect of ZnPC payload (0.2 %, 0.4 %, and 0.6 % w/w) on the phototoxicity of ZnPC-M in 2D and 3D cell cultures. **(A)** Mean ± SD relative viability (%) of TFK1, EGI1, and A431 cells incubated with increasing concentrations of ZnPC-M in fully supplemented RPMI for 6 h. Cells were illuminated at a cumulative radiant exposure of 12 J/cm^2. Data were normalized to the mean value of the control group (illuminated, non-treated cells). Fits were generated using the non-linear fit data analysis function in GraphPad Prism. **(B and C)** TFK1 spheroids cell viability following 24 h incubation with 30 μM ZnPC-M and illumination at a cumulative radiant exposure of 12 J/cm^2. **(B)** Brightfield microscopy images of non-treated and treated TFK1 spheroids. **(C)** Mean ± SD relative viability (%) of TFK1 spheroids normalized to the mean value of the control group (illuminated, non-treated spheroids).

concentration, the phototoxicity was also plotted as a function of polymer concentration in Fig. S10. In that scenario it was expected that the phototoxicity would be highest for the 0.6 % w/w ZnPC-M because a higher amount of PS would be available inside cells. However, there was no increased photodynamic effect for the higher payload at the same polymer concentration (Fig. S10). In TFK1 spheroids, which better resemble *in vivo* conditions, ZnPC-M were also able to induce phototoxicity as observed in Fig. 3B. Fig. 3C shows that the 0.2 % ZnPC-M reduced cell viability in 34 % on average, while for the 0.6 % w/w ZnPC-M the cell viability remained close to 100 %. Thus, in agreement with the 2D assays, the 0.6 % w/w ZnPC-M were the least efficient. As discussed and shown in Fig. S5, the 0.6 % ZnPC-M have the lowest capacity to generate ROS at equimolar ZnPC concentration in the culture medium, probably due to the high degree of aggregation of ZnPC (Broekgaarden, 2014). The lack of dependence of phototoxicity on increasing payloads during the 6 h drug-light interval suggests that ZnPC does not revert to the monomeric state, unlike what has been reported for liposome-delivered ZnPC (Dias, 2021; Dias, 2022). Either the ZnPC is not released efficiently from the micelles upon cellular internalization and/or the ZnPC remains aggregated after being released. In both cases, the ZnPC is not fully available for activation by light, and thus insufficient oxidative stress is generated to induce cell death. It is currently unclear what the intracellular fate is of the ZnPC-Ms following internalization. Some polymeric micelles remain intact after endocytosis (Ghezzi, 2021), with the lowering of pH in late endosomes likely fortifying the ZnPC-polymer complex. If this is indeed the case for the 0.6 % w/w ZnPC-M, there would be a significant decrease in triplet state quantum yield of ZnPC, reduced type II photochemical reactivity, and abrogated ROS production (Broekgaarden, 2014).

Corroboratively, Hofman *et al.* have reported that micelles composed of mPEG750-b-OCl$_5$ with a benzoyl terminal group and loaded with mTHPC induce higher phototoxicity when pre-incubated with lipase, indicating the importance of enzymatic degradation of the polymer for PDT efficacy (Hofman, 2008). On the other hand, monomerization of the PS inside the cells is possible, but the rate and extent of disaggregation depends strongly on the hydrophobicity of the PS; the higher the hydrophobicity, the lower the disaggregation (Kelbauskas and Dietel, 2002). The axial modification of ZnPC could be employed to reduce aggregation inside the micelles (Jing, 2018; Przybył and Janczak, 2016). On the other hand, simply reducing the loading while increasing the micelle dose is a valid strategy to reduce aggregation-induced quenching. In fact, increasing the number of injected NPs can lead to an improvement in circulation time by saturating the clearance capacity of the mononuclear phagocyte system and consequently causing a higher deposition of NPs in the tumor (Ouyang, 2020). Taking this into account, 0.2 % and 0.4 % w/w ZnPC-M are the most promising for efficient ZnPC

activation.

3.4. Nanobody-targeted micelles

Binding and subsequent cellular internalization of NPs can be enhanced by targeting ligands conjugated to the surface of NPs (Noble, 2014). The PEG backbone of micelles reduces cellular interaction due to polymer hydrophilicity, which is important for a long circulation time, but hinders uptake by cancer cells when they reach the tumor site (Mishra et al., 2004). Therefore, nanobodies directed against either MET or EGFR were grafted onto the micelle surface. This was achieved by incorporating PCL-PEG with a maleimide group (PCL-PEG-MAL) into micelles. The maleimide group can react with a nanobody through its C-terminal cysteine to form a stable covalent thioether bond (Fig. 4A).

PCL-PEG-MAL was synthesized following an in-house protocol (Fig. S11) and characterized by ^{1}H NMR and GPC (Figs. S12 and S13). Micelles with 10 % w/w of PCL-PEG-MAL were prepared encapsulating 0.4 % w/w ZnPC, which was shown above to have the highest plasma stability and phototoxicity in cells. The MET-Nbs and EGFR-Nbs were conjugated to independent micelles at a 4.5:100 Nb:PCL-PEG-MAL ratio, which was confirmed by SDS-PAGE (Fig. 4B and S14). The samples where the Nbs were added to freshly prepared micelles (lanes 3 and 5), the band appears at a higher molecular weight compared to the free Nb (lanes 2 and 4, Fig. 4B), indicating that the 15–16-kDa Nb bound to the 5-kDa PCL-PEG-MAL. No free Nb was detected for both MET- and EGFR-targeted micelles (MET-TM and EGFR-TM), attesting to a high conjugating efficiency. As expected, no Nbs were detected for the non-targeted micelles (NTM, lane 1). The average hydrodynamic diameter was approximately 90 nm for the 3 formulations (Fig. 4C), which is 30 nm larger than the values reported in Fig. 1B. This increase in size might be caused by the centrifugation step performed with Vivaspin columns during the preparation of these non-targeted and targeted micelles.

The association of the MET-TM and the EGFR-TM was compared with that of NTM by measuring ZnPC fluorescence in three cell lines with different expression of MET and EGFR on the cell surface. The MET expression is slightly higher for EGI1, and similar between TFK1 and A431, while the EGFR expression in A431 cells is 6 and 9 × higher than in TFK1 and EGI1 cells, respectively, as determined by flow cytometry (Fig. 5A). As shown in Fig. 5B, MET-TM bound more efficiently to TFK1, EGI1, and A431 cells than NTM, although the association was only statistically significant for the TFK1 and EGI1 cell lines (Table S2). The selective binding advantage was also achieved after 6 h incubation for all 3 cell lines (Fig. S15). The specific association of MET-TM with MET-expressing cells was validated with a competition assay, where cells were pre-incubated with a saturating concentration of free MET-Nb prior to exposure to micelles. Under these conditions, the association of MET-TM was decreased and similar to that of NTM for the 3 cell lines. For the EGFR-TM, the highest increase in ZnPC association (i.e., about 4-fold) compared to NTM was observed in A431 cells (Fig. 5B). This correlates with the EGFR expression that is the highest in A431 cells. The competition assay showed that the interaction of EGFR-TM is mediated by the EGFR receptor in A431 cells inasmuch as the MFI was reduced to levels similar to those of cells incubated with NTM. In TFK1 cells, the effect of the competition group was less evident.

Next, the effect of targeting on phototoxicity of ZnPC-M was evaluated and compared with the association studies (Fig. 5B, 5C, and S16). In EGI1 and A431 cells, both MET-TM and EGFR-TM were more phototoxic than NTM. The EGFR-TM induced the most profound reduction in cell viability in A431 cells, with a roughly 4-fold decrease in LC_{50} compared to NTM (Fig. 5C), which is in agreement with the 4-fold increase in ZnPC MFI value. MET-TM was the most phototoxic in EGI1 cells, however the goodness of fit (R^2) obtained was lower than in the A431 cells. Conversely, for the TFK1 cells no differences were observed between targeted and non-targeted micelles at 10 μM of ZnPC (Fig. S16). The absence of Nb-related toxicity was demonstrated in a previous study (Liu, 2020).

These data show that the association of nanobody-targeted micelles generally increases with increasing abundance of target receptors. This has also been reported for mTHPC loaded PCL-PEG micelles conjugated to anti-EGFR Nbs (Liu, 2020). However, increased phototoxicity for the formulations with the highest binding was not observed in all cases, suggesting the involvement of other factors in regard to cell death induction. The lack of enhanced phototoxicity in TFK1 cells, despite the higher association of MET-TM compared to NTM, may be because the difference in uptake of ZnPC is not large enough to induce a notable effect. In this case, adjusting the amount of Nbs per ZnPC-M might be a strategy to engage more MET receptors with MET-TM in moderately expressing cells. We have shown for liposomes conjugated with MET-Nb that the higher the density of Nbs on the surface of the nanocarrier, the stronger the association with the target receptor (Mesquita, 2022).

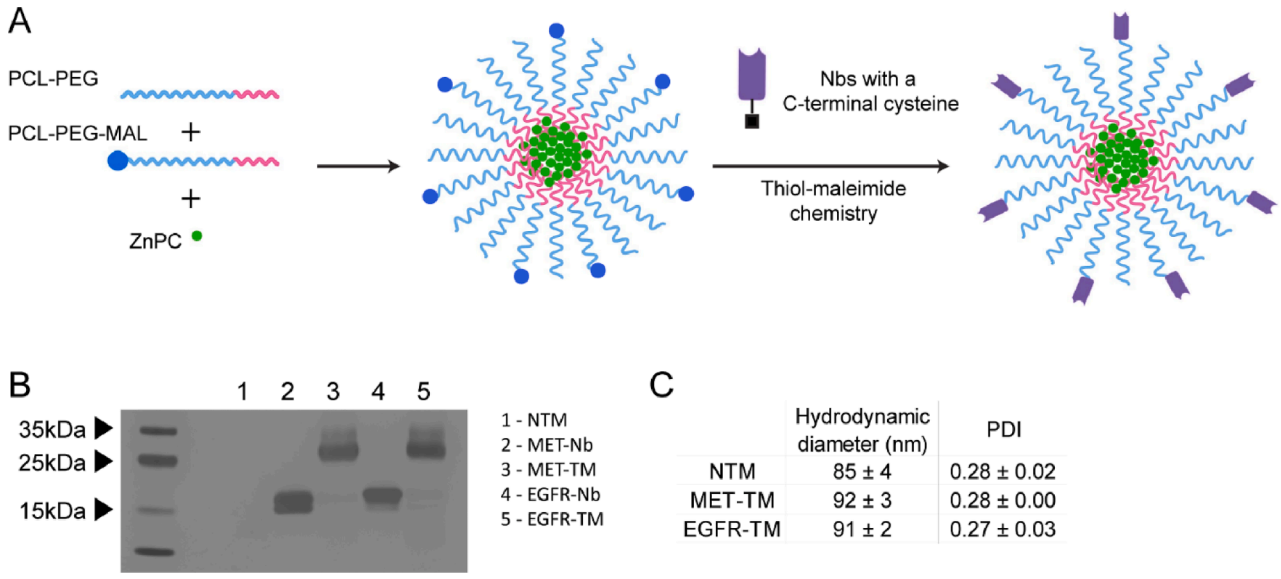

	Hydrodynamic diameter (nm)	PDI
NTM	85 ± 4	0.28 ± 0.02
MET-TM	92 ± 3	0.28 ± 0.00
EGFR-TM	91 ± 2	0.27 ± 0.03

Fig. 4. Nanobodies targeting MET or EGFR were successfully conjugated to ZnPC-M. **(A)** Schematic of nanobody-targeted micelles prepared via thiol-maleimide click chemistry. **(B)** SDS-PAGE with silver staining of 1) NTM, 2) MET-Nb, 3) MET-TM, 4) EGFR-Nb, and 5) EGFR-TM before the centrifugation step with Vivaspin columns. **(C)** Size and polydispersity of NTMs, MET-TMs and EGFR-TMs. Data represent mean ± SD (N = 3).

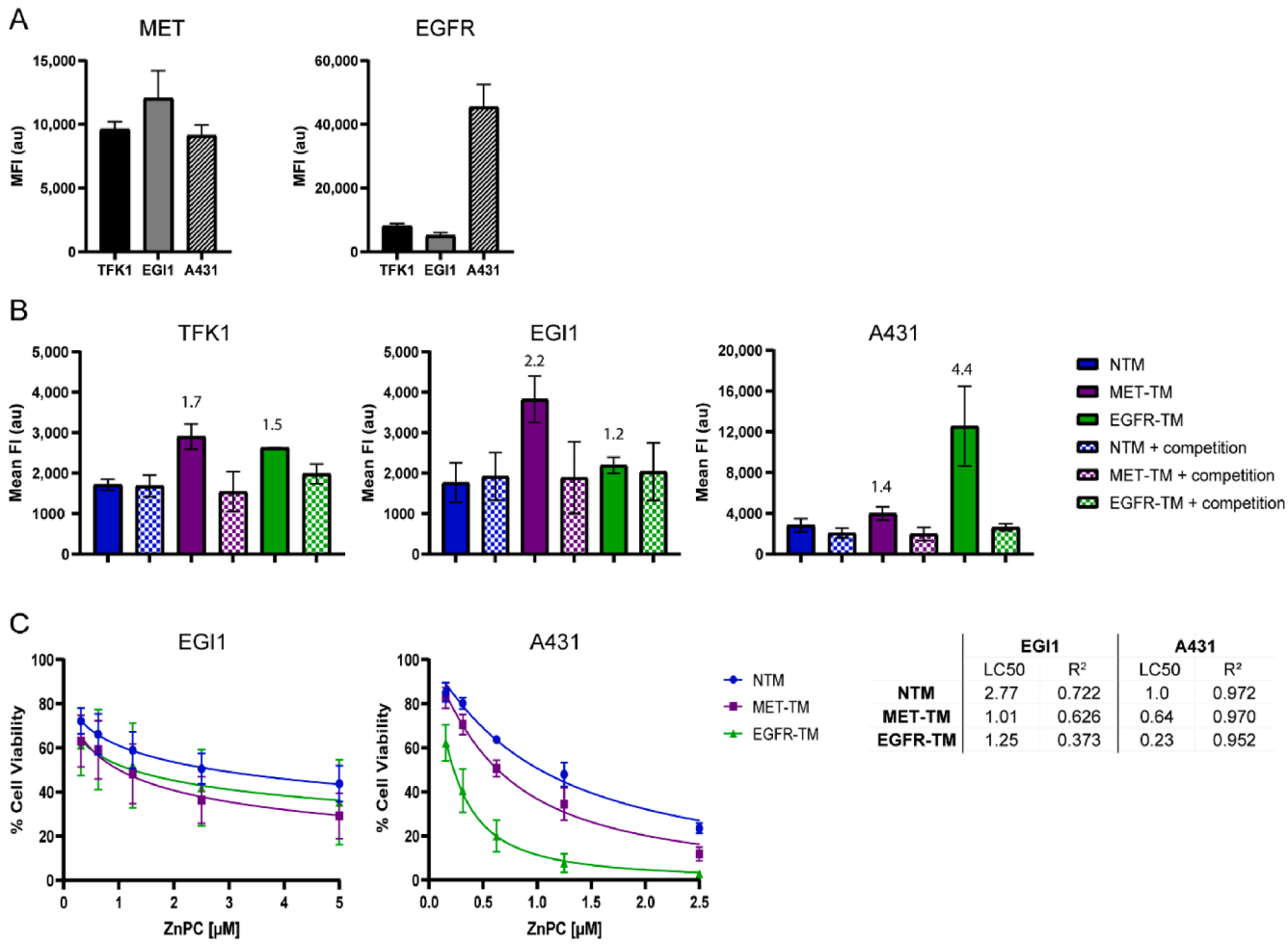

	EGI1		A431	
	LC50	R^2	LC50	R^2
NTM	2.77	0.722	1.0	0.972
MET-TM	1.01	0.626	0.64	0.970
EGFR-TM	1.25	0.373	0.23	0.952

Fig. 5. MET- and EGFR- targeted micelles (MET-TL and EGFR-TL, respectively) bind specifically to the target cells, enhancing phototoxicity. **(A)** MET and EGFR expression by TFK1, EGI1, and A431 cells measured by flow cytometry. The mean fluorescence intensity (FI) of the fluorescently labeled anti-MET or anti-EGFR antibody is plotted per cell line. **(B)** Cellular association with non-targeted micelles (NTM), MET-TM, and EGFR-TM. Cells were incubated with micelles containing a final ZnPC concentration of 2 μM for 1 h under standard culture conditions. Specific association of MET-TM and EGFR-TM was determined by a competition assay. In this case, cells were pre-incubated with a solution of 1 μM of MET-Nbs or EGFR-Nbs for 15 min, followed by incubation with NTM, MET-TM, or EGFR-TM. Micelle association was measured by flow cytometry and plotted as mean FI of ZnPC. Data were normalized to the mean of the control group (non-treated cells) and expressed as mean ± SD of 2 independent experiments (performed in duplicate). Fold-change in mean FI between MET-TM or EGFR-TM and NTM is indicated above the bar for each cell line. **(C)** Relative viability (%) of EGI-1 and A431 cells incubated for 6 h with a range of concentrations of ZnPC-M dispersed in fully supplemented RPMI. Cells were illuminated at a cumulative radiant exposure of 12 J/cm^2. Data were normalized to the mean value of the control group (illuminated, non-treated cells). Fits were generated using the non-linear fit data analysis function in GraphPad Prism. Table with the lethal concentration 50 (LC_{50}) and the goodness of fit (R^2) value calculated from each fit.

Moreover, Woythe *et al.* have reported that increasing the valency of anti-EGFR aptamers in aptamer-functionalized silica-supported lipid bilayers has higher impact on cells with low-to-intermediate expression of EGFR than high expression (Woythe, 2023).

Our group has previously tested PCL-PEG micelles conjugated to an EGFR-Nb, although the micelles were loaded with mTHPC instead of ZnPC. In A431 cells, ZnPC-loaded EGFR-TM yielded an LC_{50} of 0.23 μM at 12 J/cm^2, while the mTHPC formulation was associated with an LC_{50} of 14.7 μM at 2.1 J/cm^2, demonstrating the higher potency of ZnPC (Liu, 2020). Other types of ligands are being explored to increase the uptake of photosensitizer molecules by cancer cells. For example, Master *et al.* have conjugated an EGFR-targeting peptide to PCL-PEG micelles encapsulating silicon phthalocyanine. However, an advantage over non-targeted micelles was only observed for the 1 h incubation time point, while after 5 h and 24 h incubation no significant differences were observed. PEG-poly(L-lactide) micelles functionalized with folic acid and loaded with ZnPC were more phototoxic than the non-targeted counterpart (i.e., halving of the LC_{50}) in Me45 and SKOV3 cells after 24 h incubation, with the effect increasing with increasing amounts of folic acid (Lamch, 2019). On the other hand, decorating mTHPC-encapsulating liposomes with transferrin has not been proved beneficial to PDT efficacy in esophageal adenocarcinoma (OE21) cells expressing transferrin receptor (Paszko, 2013). This is possibly due to a premature release of mTHPC and highlights the importance of finding a suitable nanocarrier with high stability for each photosensitizer. While decreased circulation time have been reported for ligand-targeted nanocarriers compared to non-targeted counterparts (McNeeley et al., 2007), previous research from our group has demonstrated that the pharmacokinetics of PCL-PEG micelles is not negatively affected by the conjugation of Nbs (Liu, 2020). Moreover, we have shown that adjusting the density of MET-Nb conjugated to liposomes can preserve the stealthiness capabilities provided by PEG, thus reducing the interaction with phagocytic cells (Mesquita, 2022).

4. Conclusions

We investigated the suitability of micelles composed of poly(ε-caprolactone)-b-poly(ethylene) glycol (PCL-PEG) copolymer as

nanocarriers for ZnPC-PDT of solid tumors. The ZnPC:polymer ratio (i.e., payload) was found to affect the ability of ZnPC to produce ROS and consequently kill cells upon photoactivation. The ZnPC-M with the lower payloads (0.2 and 0.4 % w/w) were the most stable in human plasma, with minimal redistribution to HDL, and induced the highest phototoxicity. Aggregation of ZnPC in the micelle core is possibly the cause of the reduced phototoxicity at the highest payloads. Accordingly, an optimal payload per PS/nanocarrier combination needs to be defined as the PS must be in monomeric form to be active – a phenomenon that is relevant for these micelles but not for other nanoparticulate photosensitizer delivery systems such as liposomes. Furthermore, the conjugation of nanobodies (Nb) targeting MET or EGFR to the surface of micelles generally enhanced the association and phototoxicity in cells expressing the target receptor. However, the benefit of a targeting ligand is cell type-dependent and relies on other factors than target expression alone. A better understanding of these factors will improve the design of Nb-targeting micelles, which in turn will translate to augmented PDT efficacy.

Funding

The work of Bárbara Mesquita is supported by the Portuguese Foundation: Fundação para a Ciência e a Tecnologia (FCT) grant SFRH/BD/140283/2018. Michal Heger was supported by grants from the Dutch Cancer Foundation (KWF project # 10666), a Zhejiang Provincial Foreign Expert Program Grant, and the Zhejiang Provincial Key Natural Science Foundation of China (#Z20H160031).

CRediT authorship contribution statement

Bárbara Mesquita: Writing – original draft, Visualization, Methodology, Investigation, Funding acquisition, Formal analysis, Data curation. **Arunika Singh:** Investigation, Formal analysis. **Cèlia Prats Masdeu:** Investigation, Formal analysis. **Nienke Lokhorst:** Investigation, Formal analysis. **Erik R. Hebels:** Methodology, Investigation, Formal analysis. **Mies van Steenbergen:** Methodology, Investigation, Formal analysis. **Enrico Mastrobattista:** Writing – review & editing. **Michal Heger:** Writing – review & editing, Supervision, Resources, Conceptualization. **Cornelus F. van Nostrum:** Writing - review and editing, Supervision, Conceptualization. **Sabrina Oliveira:** Writing – review & editing, Supervision, Resources, Project administration, Conceptualization.

Declaration of competing interest

The authors declare that they have no known competing financial interests or personal relationships that could have appeared to influence the work reported in this paper.

Data availability

Data will be made available on request.

Acknowledgments

We are thankful to Yunlei Li (Department of Pathology and Clinical Bioinformatics, Erasmus Medical Center) for advise on statistical analysis of flow cytometry data, to Francesco Palmieri (Department of Pharmaceutics, Utrecht Institute for Pharmaceutical Sciences, Utrecht University) for the advice on PCL-PEG-MAL synthesis and purification, and to Antoinette van den Dikkenberg (Department of Pharmaceutics, Utrecht Institute for Pharmaceutical Sciences, Utrecht University) for helping with GPC and DSC measurements.

Appendix A. Supplementary data

Supplementary data to this article can be found online at https://doi.org/10.1016/j.ijpharm.2024.124004.

References

Allen, C.M., Sharman, W.M., Van Lier, J.E., 2001. Current status of phthalocyanines in the photodynamic therapy of cancer. J. Porphyrins Phthalocyanines 5 (02), 161–169.
Ashford, M.B., England, R.M., Akhtar, N., 2021. Highway to success—developing advanced polymer therapeutics. Adv. Ther. 4 (5), 2000285.
Bhattacharjee, S., 2016. DLS and zeta potential–what they are and what they are not? J. Control. Release 235, 337–351.
Bilardo, R., et al., 2022. Influence of surface chemistry and morphology of nanoparticles on protein corona formation. Wiley Interdiscip. Rev. Nanomed. Nanobiotechnol. 14 (4), e1788.
Broadwater, D., et al., 2021. Current advances in photoactive agents for cancer imaging and therapy. Annu. Rev. Biomed. Eng. 23, 29–60.
Broekgaarden, M., et al., 2014. Development and in vitro proof-of-concept of interstitially targeted zinc-phthalocyanine liposomes for photodynamic therapy. Curr. Med. Chem. 21 (3), 377–391.
Cabral, H., et al., 2018. Block copolymer micelles in nanomedicine applications. Chem. Rev. 118 (14), 6844–6892.
Castano, A.P., Demidova, T.N., Hamblin, M.R., 2004. Mechanisms in photodynamic therapy: part one—photosensitizers, photochemistry and cellular localization. Photodiagn. Photodyn. Ther. 1 (4), 279–293.
Cramer, G.M., Cengel, K.A., Busch, T.M., 2022. Forging forward in photodynamic therapy. Cancer Res. 82 (4), 534–536.
Dias, L.M., et al., 2021. Attritional evaluation of lipophilic and hydrophilic metallated phthalocyanines for oncological photodynamic therapy. J. Photochem. Photobiol. B Biol. 216, 112146.
Dias, L.M., et al., 2022. Metallated phthalocyanines and their hydrophilic derivatives for multi-targeted oncological photodynamic therapy. J. Photochem. Photobiol. B Biol. 234, 112500.
Ghezzi, M., et al., 2021. Polymeric micelles in drug delivery: an insight of the techniques for their characterization and assessment in biorelevant conditions. J. Control. Release 332, 312–336.
Hofman, J.-W., et al., 2008. Photocytotoxicity of mTHPC (temoporfin) loaded polymeric micelles mediated by lipase catalyzed degradation. Pharm. Res. 25, 2065–2073.
Hopper, C., Niziol, C., Sidhu, M., 2004. The cost-effectiveness of Foscan mediated photodynamic therapy (Foscan-PDT) compared with extensive palliative surgery and palliative chemotherapy for patients with advanced head and neck cancer in the UK. Oral Oncol. 40 (4), 372–382.
Huang, Y.-Y., et al., 2012. Can nanotechnology potentiate photodynamic therapy? Nanotechnol. Rev. 1 (2), 111–146.
Isele, U., et al., 1994. Large-scale production of liposomes containing monomeric zinc phthalocyanine by controlled dilution of organic solvents. J. Pharm. Sci. 83 (11), 1608–1616.
Jing, C., et al., 2018. Axial modification inhibited H-aggregation of phthalocyanines in polymeric micelles for enhanced PDT efficacy. Chem. Commun. 54 (32), 3985–3988.
Kelbauskas, L., Dietel, W., 2002. Internalization of aggregated photosensitizers by tumor cells: Subcellular time-resolved fluorescence spectroscopy on derivatives of pyropheophorbide-a ethers and chlorin e6 under Femtosecond one-and two-photon excitation. Photochem. Photobiol. 76 (6), 686–694.
Klibanov, A.L., et al., 1990. Amphipathic polyethyleneglycols effectively prolong the circulation time of liposomes. FEBS Lett. 268 (1), 235–237.
Lambert, J.M., Morris, C.Q., 2017. Antibody–drug conjugates (ADCs) for personalized treatment of solid tumors: a review. Adv. Ther. 34, 1015–1035.
Lamch, Ł., et al., 2019. Folate-directed zinc (II) phthalocyanine loaded polymeric micelles engineered to generate reactive oxygen species for efficacious photodynamic therapy of cancer. Photodiagn. Photodyn. Ther. 25, 480–491.
Larroque, C., Pelegrin, A., Van Lier, J., 1996. Serum albumin as a vehicle for zinc phthalocyanine: photodynamic activities in solid tumour models. Br. J. Cancer 74 (12), 1886–1890.
Li, X., et al., 2020. Clinical development and potential of photothermal and photodynamic therapies for cancer. Nat. Rev. Clin. Oncol. 17 (11), 657–674.
Liu, Y., et al., 2020. EGFR-targeted nanobody functionalized polymeric micelles loaded with mTHPC for selective photodynamic therapy. Mol. Pharm. 17 (4), 1276–1292.
Master, A.M., et al., 2012. Optimization of a nanomedicine-based silicon phthalocyanine 4 photodynamic therapy (Pc 4-PDT) strategy for targeted treatment of EGFR-overexpressing cancers. Mol. Pharm. 9 (8), 2331–2338.
McFarland, S.A., et al., 2020. Metal-based photosensitizers for photodynamic therapy: the future of multimodal oncology? Curr. Opin. Chem. Biol. 56, 23–27.
McNeeley, K.M., Annapragada, A., Bellamkonda, R.V., 2007. Decreased circulation time offsets increased efficacy of PEGylated nanocarriers targeting folate receptors of glioma. Nanotechnology 18 (38), 385101.
Mesquita, B.S., et al., 2022. The impact of nanobody density on the Targeting efficiency of PEGylated liposomes. Int. J. Mol. Sci. 23 (23), 14974.
Min, H.-Y., Lee, H.-Y., 2022. Molecular targeted therapy for anticancer treatment. Exp. Mol. Med. 54 (10), 1670–1694.
Mishra, S., Webster, P., Davis, M.E., 2004. PEGylation significantly affects cellular uptake and intracellular trafficking of non-viral gene delivery particles. Eur. J. Cell Biol. 83 (3), 97–111.

Miyamoto, M., et al., 2011. Prognostic significance of overexpression of c-Met oncoprotein in cholangiocarcinoma. Br. J. Cancer 105 (1), 131–138.
Muyldermans, S., 2013. Nanobodies: natural single-domain antibodies. Annu. Rev. Biochem. 82, 775–797.
Noble, G.T., et al., 2014. Ligand-targeted liposome design: challenges and fundamental considerations. Trends Biotechnol. 32 (1), 32–45.
Nunes, S., Sguilla, F., Tedesco, A.C., 2004. Photophysical studies of zinc phthalocyanine and chloroaluminum phthalocyanine incorporated into liposomes in the presence of additives. Braz. J. Med. Biol. Res. 37, 273–284.
Obata, M., et al., 2018. RAFT synthesis of polystyrene-block-poly (polyethylene glycol monomethyl ether acrylate) for zinc phthalocyanine-loaded polymeric micelles as photodynamic therapy photosensitizers. J. Polym. Sci. A Polym. Chem. 56 (5), 560–570.
Obata, M., et al., 2021. Effect of the hydrophobic segment of an amphiphilic block copolymer on micelle formation, zinc phthalocyanine loading, and photodynamic activity. Eur. Polym. J. 147, 110325.
Ochsner, M., 1996. Light scattering of human skin: a comparison between zinc (II)—phthalocyanine and photofrin II®. J. Photochem. Photobiol. B Biol. 32 (1–2), 3–9.
Ouyang, B., et al., 2020. The dose threshold for nanoparticle tumour delivery. Nat. Mater. 19 (12), 1362–1371.
Park, J., et al., 2021. Current limitations and recent progress in nanomedicine for clinically available photodynamic therapy. Biomedicines 9 (1), 85.
Paszko, E., et al., 2013. Transferrin conjugation does not increase the efficiency of liposomal Foscan during in vitro photodynamic therapy of oesophageal cancer. Eur. J. Pharm. Sci. 48 (1–2), 202–210.
Plaetzer, K., et al., 2009. Photophysics and photochemistry of photodynamic therapy: fundamental aspects. Lasers Med. Sci. 24, 259–268.
Polo, L., et al., 1992. The distribution of the tumour photosensitizers Zn (II)-phthalocyanine and Sn (IV)-etiopurpurin among rabbit plasma proteins. Cancer Lett. 66 (3), 217–223.
Przybył, B., Janczak, J., 2016. Complexes of zinc phthalocyanine with monoaxially coordinated imidazole-derivative ligands. Dyes Pigm. 130, 54–62.
Quattrini, F., et al., 2021. Asymmetric flow field-flow fractionation as a multifunctional technique for the characterization of polymeric nanocarriers. Drug Deliv. Transl. Res. 11, 373–395.
Raghav, K.P., et al., 2012. cMET and phospho-cMET protein levels in breast cancers and survival outcomes. Clin. Cancer Res. 18 (8), 2269–2277.
Roguin, L.P., et al., 2019. Zinc (II) phthalocyanines as photosensitizers for antitumor photodynamic therapy. Int. J. Biochem. Cell Biol. 114, 105575.
Santos, L.L., et al., 2018. Treatment of head and neck cancer with photodynamic therapy with redaporfin: a clinical case report. Case Rep. Oncol. 11 (3), 769–776.
Suk, J.S., et al., 2016. PEGylation as a strategy for improving nanoparticle-based drug and gene delivery. Adv. Drug Deliv. Rev. 99, 28–51.
Van Straten, D., et al., 2017. Oncologic photodynamic therapy: basic principles, current clinical status and future directions. Cancers 9 (2), 19.
Varela-Moreira, A., et al., 2017. Clinical application of polymeric micelles for the treatment of cancer. Mater. Chem. Front. 1 (8), 1485–1501.
Wagner, M., et al., 2014. Asymmetric flow field-flow fractionation in the field of nanomedicine. Anal. Chem. 86 (11), 5201–5210.
Weijer, R., et al., 2015. Enhancing photodynamic therapy of refractory solid cancers: combining second-generation photosensitizers with multi-targeted liposomal delivery. J. Photochem. Photobiol. C: Photochem. Rev. 23, 103–131.
Woythe, L., et al., 2023. Valency and affinity control of aptamer-conjugated nanoparticles for selective cancer cell targeting. J. Control. Release 355, 228–237.
Yao, H.-P., Hudson, R., Wang, M.-H., 2020. Progress and challenge in development of biotherapeutics targeting MET receptor for treatment of advanced cancer. biochimica et biophysica acta (BBA)-reviews on. Cancer 1874 (2), 188425.
Yu, Y., et al., 2023. Photodynamic therapy combined with systemic chemotherapy for unresectable extrahepatic cholangiocarcinoma: a systematic review and meta-analysis. Photodiagn. Photodyn. Ther., 103318